Breaking wave simulations by a new $k-l$ turbulence model

FRANCESCO GALLERANO, BENEDETTA IELE, FEDERICA PALLESCHI, GIOVANNI CANNATA
Department of Civil, Constructional and Environmental Engineering Sapienza University of Rome Rome, ITALY

Abstract: The three-dimensional motion equations are used to simulate the wave and velocity fields. These equations are written in integral contravariant form on a time-dependent curvilinear coordinate system. In this paper a new $\boldsymbol{k-l}$ turbulence model in contravariant form is proposed for three-dimensional simulation of breaking waves. In this model the mixing length is defined as a function of the first and second spatial derivatives of the maximum water surface elevation.

Keywords: Wave breaking; turbulence model; turbulent kinetic energy; boundary layer; boundary conditions.

Received: May 29, 2021. Revised: June 18, 2022. Accepted: July 17, 2022. Published: September 13, 2022.

1. Introduction

In the literature one of the most used turbulence models for the simulations of the breaking waves [1],[2],[3], [4],[5] and turbulent phenomena is the Smagorinsky model. This model is characterized by the presence of the Smagorinsky coefficient, which is defined (in the previous paper) without distinction in the shoaling zone, in the region around the breaking point and in the surf zone. In the models present in the literature the turbulent phenomena are underestimated by the Smagorinsky model and the dissipation of the averaged motion is due to the numerical scheme.

Another commune turbulence model used in the literature in the context of wave breaking [6],[7] is the $k-l$ model (k is the turbulent kinetic energy and l is the mixing length), in which there is no distinction of the representation of the production and dissipation of the turbulent kinetic energy before and after the breaking point.

In the simulations presented in the literature, both the abovementioned models do not take into account the turbulent phenomena at the bottom boundary layer (buffer layer and turbulent core), because the first calculation grid cell is outside the boundary layer, where these phenomena are dominant.

In this paper a new $k-l$ is proposed that is able to dissipate the average motion energy and overcomes the limitations of the abovementioned turbulence model present in the literature. To take into account the different behavior of the turbulence in the wave propagation, the mixing length is a function of the first and second spatial derivatives of the maximum water surface elevation.

In this numerical model the Navier-Stokes equations, written in integral contravariant form, expressed in a generalized time-dependent curvilinear coordinate system in
which the vertical coordinate moves following the free surface, are numerically solved. The numerical scheme uses 5th order WTENO (Wave Targeted Essentially Non-Oscillatory) reconstruction technique (from the cell average value of the variables to the point ones) and an Exact Riemann Solver. The WTENO technique is collocated in the context of the TENO and ENO reconstruction technique [8],[9], but applicated to the waves. The Poisson equation and the motion equations are expressed in terms of the conserved variables (Hu^l e H).

2. Motion Equations

The three-dimensional Navier-Stokes equations without the Christoffel symbols and the equation relative to the movement of the free surface are expressed in integral contravariant form in a time-dependent curvilinear coordinate system, that adopt conserved variables H e Hu^s $(s = 1,3)$, and are given by

$$\frac{\partial \overline{Hu^s}}{\partial \tau} = -\frac{\Delta t}{\Delta V_0 \sqrt{g_0}} \sum_{\alpha=1}^{3} \left\{ \int_{\Delta A_0^{\alpha+}} \left[\vec{\tilde{g}}^{(s)} \cdot \vec{g}_{(k)} (Hu^k) \left((Hu^\alpha / H) - v^\alpha \right) + \vec{\tilde{g}}^{(s)} \cdot \vec{g}^{(\alpha)} G(\eta H) \right] \sqrt{g_0} d\xi^\beta d\xi^\gamma - \int_{\Delta A_0^{\alpha-}} \left[\vec{\tilde{g}}^{(s)} \cdot \vec{g}_{(k)} (Hu^k) \left((Hu^\alpha / H) - v^\alpha \right) + \vec{\tilde{g}}^{(s)} \cdot \vec{g}^{(\alpha)} G(\eta H) \right] \sqrt{g_0} d\xi^\beta d\xi^\gamma \right\} + \tag{1}$$

$$\frac{\partial \overline{H}}{\partial \tau} = \frac{1}{\Delta A_0^3 \sqrt{g_0}} \sum_{\alpha=1}^{2} \left[\int_0^1 \int_{\Delta \xi_0^{\alpha+}} Hu^\alpha \sqrt{g_0} d\xi^\beta d\xi^3 - \int_0^1 \int_{\Delta \xi_0^{\alpha-}} Hu^\alpha \sqrt{g_0} d\xi^\beta d\xi^3 \right] \tag{2}$$

The transformation from the Cartesian coordinate system (x^1, x^2, x^3, t) to the curvilinear one $(\xi^1, \xi^2, \xi^3, \tau)$ is given by

$$\xi^1 = \xi^1(x^1, x^2, x^3); \ \xi^2 = \xi^2(x^1, x^2, x^3); \ \xi^3 = \frac{x^3 + h(x^1, x^2)}{H(x^1, x^2, t)}; t = \tau \tag{3}$$

In (3) h in the undisturbed water depth, $H(x^1,x^2,t) = h(x^1,x^2) + \eta(x^1,x^2,t)$ is the total water depth and η is the free surface elevation with respect to the undisturbed water depth. In (1) and (2) $\overline{Hu^s}$ and $\overline{H}$ are the cell average values of the conserved variables. u^s ($s = 1,3$) and v^α ($\alpha = 1,3$) are respectively the contravariant components of the fluid velocity and the velocity of the moving coordinates. $\vec{g}_{(l)} = \partial\vec{x}/\partial\xi^l$ and $\vec{g}^{(l)} = \partial\xi^l/\partial\vec{x}$ are the contravariant and covariant base vectors. $\sqrt{g} = H\sqrt{g_0}$, in which $\sqrt{g_0} = \vec{k}\cdot\left(\vec{g}_{(1)}\wedge\vec{g}_{(2)}\right)$, $\vec{k}$ indicates the vertical unit vector and $\wedge$ indicates the vector product is the Jacobian of the transformation. $\vec{g}^{(l)}$ is the covariant base vector defined at the center of the control volume. The volume $V_0 = \Delta\xi^1\Delta\xi^2\Delta\xi^3$ and the areas $\Delta A_0^\alpha = \Delta\xi^\beta\Delta\xi^\gamma$ are not time dependent. The boundary surfaces of the control volume ΔV_0, on which the coordinate ξ^α is constant, that surfaces are in correspondence of the larger and smaller value of ξ^α (α, β and γ are cyclic), are $\Delta A_0^{\alpha+}$ and $\Delta A_0^{\alpha-}$. the contour lines of the surface element $\Delta A_o^3 = \Delta\xi^1\Delta\xi^2$, on which ξ^α is constant and are located respectively in correspondence of the larger and smaller value of ξ^α, are $\Delta\xi_o^{\alpha+}$ e $\Delta\xi_o^{\alpha-}$ (with $\alpha = 1,2$). $TR^{k\alpha}$ are the contravariant components of the stress tensor that contains the dynamic pressure term, ρ is the fluid density and G is the gravity acceleration.

For obtaining a divergence-free velocity field the advancing in time of the numerical solution a predictor-corrector procedure is used. To an approximated not divergence-free velocity field $(Hu^s)^*$ is added a corrector divergence-free velocity field, $(Hu^s)^C$, that takes into account the dynamic pressure.

$$(Hu^s)^C = g^{sk}H\left(\frac{\partial\Psi}{\partial s}\right) \tag{4}$$

Ψ is the potential scalar, obtained by the solution of the Poisson equation given by

$$\frac{\partial\left(g^{sk}\frac{\partial\Psi}{\partial\xi^s}H\sqrt{g_0}\right)}{\partial\xi^k} = -\frac{\partial(Hu^s)^*\sqrt{g_0}}{\partial\xi^s} \tag{5}$$

3. Turbulence Model

In the following paragraph the Smagorinsky model is presented and the new proposed $k-l$ model is explained.

3.1 Smagorinsky Turbulence Model

Many authors [1],[2],[3],[4],[5] use Smagorinsky model to represent the turbulence in the breaking waves. In turbulent stress tensor, $T^{lm} = -2\nu_t\, S^{lm}$, where S^{lm} is the strain rate tensor, the turbulent eddy viscosity is given by

$$\nu_T = (C_S\Delta)^2|S^{lm}| \tag{6}$$

$\Delta = \sqrt[3]{\Delta x\Delta y\Delta z}$ is the dimension of the grid size and C_S is the abovementioned Smagorinsky coefficient.

In the lower part, close to the bottom, and in the higher part of the boundary layer there is the dominance respectively of viscous stresses and turbulent stresses. In the middle part of the boundary layer viscous and turbulent stresses coexist.

The motion equations, in which turbulent stress tensor is modelled by Smagorinsky, are solved in the turbulent core. In this model in the turbulent boundary layer the turbulent eddy viscosity is given by

$$\nu_T = \kappa u^* z \tag{7}$$

in which $\kappa = 0.41$ is the von Kàrmàn constant.

3.2 $k-l$ Turbulence Model

In the $k-l$ model, in which k is the turbulent kinetic energy and l is the mixing length, the turbulent kinetic energy equation is solved. This equation is expressed in integral contravariant form in a time-dependent curvilinear coordinate system.

$$\begin{aligned}
\frac{\partial\overline{Hk}}{\partial\tau} = \\
-\frac{1}{\Delta V_0\sqrt{g_0}}\sum_{\alpha=1}^{3}\left\{\int_{\Delta A_0^{\alpha+}}[Hk(u^\alpha - v^\alpha)]\sqrt{g_0}d\xi^\beta d\xi^\gamma - \int_{\Delta A_0^{\alpha-}}[Hk(u^\alpha - v^\alpha)]\sqrt{g_0}d\xi^\beta d\xi^\gamma\right\} \\
+\frac{1}{\Delta V_0\sqrt{g_0}}\sum_{\alpha=1}^{3}\left\{\int_{\Delta A_0^{\alpha+}}\left[(\nu + \nu_T)g^{\alpha r}\frac{\partial k}{\partial\xi^r}H\sqrt{g_0}\right]d\xi^\beta d\xi^\gamma - \right. \\
\left.\int_{\Delta A_0^{\alpha+}}\left[(\nu+\nu_T)g^{\alpha r}\frac{\partial k}{\partial\xi^r}H\sqrt{g_0}\right]d\xi^\beta d\xi^\gamma\right\} + \\
\frac{1}{\Delta V_0\sqrt{g_0}}\int_{\Delta V_0}PH\sqrt{g_0}d\xi^\beta d\xi^\gamma + \frac{1}{\Delta V_0\sqrt{g_0}}\int_{\Delta V_0}\varepsilon H\sqrt{g_0}d\xi^\beta d\xi^\gamma
\end{aligned} \tag{8}$$

in which $\varepsilon = C_\mu\, k^{\frac{3}{2}}/l$ is the dissipation of turbulent kinetic energy, P is the production of turbulent kinetic energy. The turbulent eddy viscosity is given by

$$\nu_T = C_\mu\sqrt{k}l \text{ with } C_\mu = 0.09 \tag{9}$$

In the new $k-l$ model the mixing length is a function of the first and second spatial derivatives of the maximum water surface elevation, $\partial\eta_{max}(\xi^1)/\partial\xi^1$ and $\partial^2\eta_{max}(\xi^1)/(\partial\xi^1)^2$. Let $\lambda_{max}(\xi^1) = \eta_{max}(\xi^1) + \eta_{min}(\xi^1)$ be the maximum wave height point by point in the time; $H_{max}(\xi^1) = \eta_{max}(\xi^1) + h(\xi^1)$ be the maximum total water depth point by point in the time; $\eta_{max}(\xi^1) = \max_t\eta(\xi^1,t)$ and $\eta_{min}(\xi^1) = \min_t\eta(\xi^1,t)$ be respectively the maximum and minimum water surface elevation.

$$l = A1\left\{1 - \frac{1}{3}[A2\ A3\ A4]\right\} * h \tag{10}$$

in which the coefficients

$$\begin{aligned}
A_1 = \lambda_{max}(\xi^1)/4H_{max}(\xi^1); \\
A_2 = \left(\frac{\partial\eta_{max}(\xi^1)}{\partial\xi^1} - \left|\frac{\partial\eta_{max}(\xi^1)}{\partial\xi^1}\right|\right)/\left(\left|\frac{\partial\eta_{max}(\xi^1)}{\partial\xi^1}\right|\right); \\
A_3 = \eta_{max}(\xi^1)/\max_{\xi^1}\eta_{max}(\xi^1);
\end{aligned} \tag{11}$$

$$A_4 = \left| \frac{\left(\frac{\partial^2 \eta_{max}(\xi^1)}{(\partial \xi^1)^2} - \left| \frac{\partial^2 \eta_{max}(\xi^1)}{(\partial \xi^1)^2} \right| \right)}{\left(2 \left| \frac{\partial^2 \eta_{max}(\xi^1)}{(\partial \xi^1)^2} \right| \right)} \right|$$

are the multiplier of the undisturbed water depth h.

The first derivative, $\partial \eta_{max}(\xi^1)/\partial \xi^1$, allows to differentiate the behavior of the turbulence model before, after and around the breaking point. Before the breaking point this derivative is positive and after is negative. The effects of the diffusive terms in the motion direction of the momentum can be reduced in the zone immediately after the breaking point by this new mixing length.

Let define two different configurations for the boundary conditions of this model.

The main difference between the two configurations is that the second configuration solves the motion equations and the turbulent kinetic energy equation also in the buffer layer unlike the first configuration. In the first configuration these equations are solved in the turbulent core. Between the buffer layer and the turbulent core, it is known that the balance between production and dissipation of turbulent kinetic energy is valid [10],[11]. The boundary conditions for the first configuration are given by the (7) for the turbulent eddy viscosity and for the turbulent kinetic energy outside the buffer layer is

$$k = \frac{u^{*2}}{C_\mu} \tag{12}$$

The turbulent phenomena and the distribution of the turbulent kinetic energy is influenced by the production of turbulent kinetic energy, in the buffer layer and the turbulent core of the bottom boundary layer this production is high.

The second configuration is characterized by the fact that the motion equations and the turbulent kinetic energy equation is solved also in the buffer layer (near the viscous sublayer), as already said, to correctly represent the strong variability of the production of turbulent kinetic energy closer to the bottom. The boundary condition for the turbulent kinetic energy is zero to the bottom, the turbulent eddy viscosity and the mixing length in the boundary layer are given respectively by (7) and (13).

$$l = \frac{\kappa u^* z}{C_\mu \sqrt{k}} \tag{13}$$

4. Results

In this paragraph the numerical results obtained with two different turbulence models are compared with the experimental ones obtained by Ting and Kirby [12] to validate the new model. The case study consists in a spilling breaker wave on a slope channel. The channel is represented in Fig. 2. The parameters of the cnoidale wave reproduced are: undisturbed water dept of $h = 0.40m$, initial wave height $H_s = 0.125m$ and period $T = 2s$. The simulations are made by 512 grid points with $\Delta x = 0.05m$ and 13 layers in vertical direction (Fig. 1).

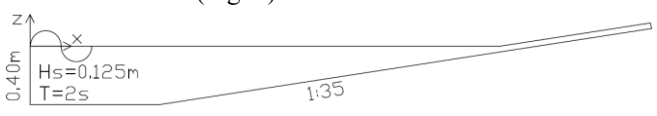

Fig. 1. Computational domain for simulation of Ting and Kirby's test case [12].

It has been considered three configurations.

In the first configuration, named C1, Smagorinsky turbulence model is adopted. The first calculation grid cell for the motion equations is in the turbulent core. The velocity boundary condition and the eddy viscosity in (7) are placed at the border between the buffer layer and the turbulent core, $y^+ = 30$ (y^+ is the adimensionless wall distance, z, u^* and ν are the vertical distance away from the wall, the bottom friction velocity calculated by a logarithmic law [11] and the kinetic viscosity coefficient).

In the second configuration, named C2, the new $k - l$ turbulence model is adopted. In this configuration, the first calculation grid cell in which the motion equations are solved, is in the turbulent core, and the lower face of this cell is at the border between the buffer layer and the turbulent core, $y^+ = 30$. The velocity boundary condition is assigned identically to the ones in C1. In addition, the boundary condition for the turbulent kinetic energy (12) is placed at the upper part of the turbulent core, $y^+ = 90$.

The third configuration, named C3, uses the new $k - l$ turbulence model, but the lower face of the first calculation grid cell is placed at the border between the viscous sublayer and the buffer layer, $y^+ = 10$. The first calculation grid cell for the motion equations and for the turbulent kinetic energy equation is in the buffer layer.

The numerical results obtained with the configuration C1 are shown in Fig. 2

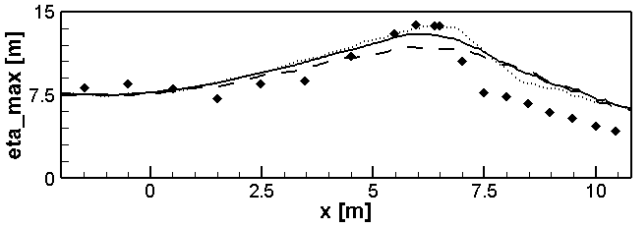

Fig. 2. Configuration C1: maximum water surface elevation. Numerical results (dotted line C_s = 0.1, solid line C_s = 0.2, dashed line C_s = 0.3) and experimental measurements (square) [12].

The breaking point has various positions in the three simulations obtained with different Smagorinsky coefficients; it is postponed in the blue line and it is anticipated in the red one. The maximum water surface elevation is overestimated in the simulation obtained with $C_s = 0.1$ (blue line) and it is underestimated in the one obtained with $C_s = 0.3$ (red line). The dissipation of the energy of the averaged motion is greater in the simulations with a high value of the Smagorinsky coefficient ($C_s = 0.3$, red solid line) and is lower in the ones with a small value of the same coefficient ($C_s = 0.1$, blue solid line). The increase of the Smagorinsky coefficient produced an increase of the turbulent eddy viscosity that reduces the wave height, because the diffusion in the motion direction of the momentum is greater. It is evident that the abovementioned coefficient influences a lot the numerical simulations and the prediction of the turbulent phenomena in the surf zone.

To overcome the limitation of the Smagorinsky model a new $k - l$ turbulence model is presented, the numerical simulations of which produced the following results. In Fig. 3

the numerical results obtained in the configuration C2 are compared with the experimental ones.

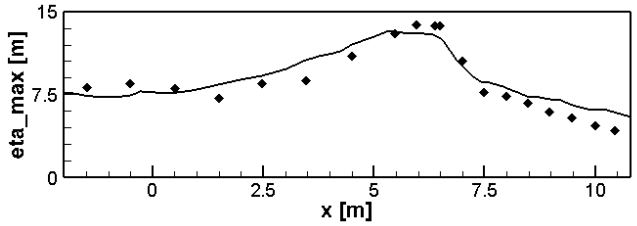

Fig. 3. Configuration C2: maximum water surface elevation. Numerical results solid line and experimental measurements (square) [12].

The new model overcomes the limitations of the Smagorinsky model. By comparing the results in Fig. 2 and Fig. 3, it can be noticed that the new $k-l$ model well predicts the breaking point and slightly underestimates the maximum water surface elevation around the breaking point. The steepness of the black line immediately after the breaking point is in good accordance with the experimental results, because the mixing length in this zone is reduced and so reduces the diffusion in the motion direction of the momentum.

The time mean turbulent kinetic energy profiles at $x = 7.27m$ e $x = 7.88m$, obtained in the configuration C2, are shown in Fig. 4.

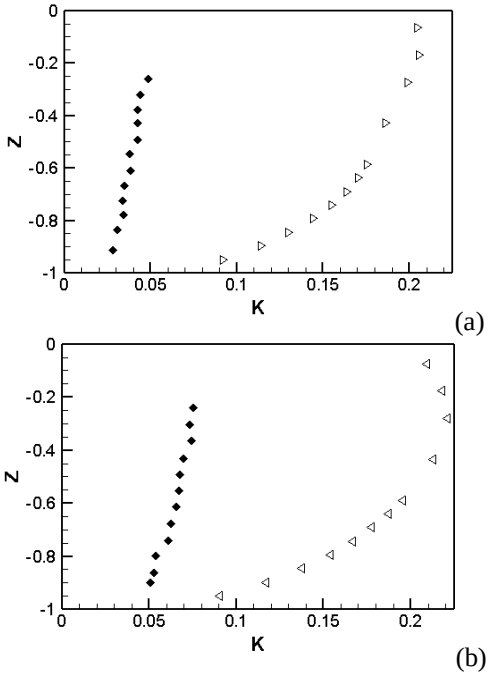

Fig. 4. Configuration C2: vertical distribution of the time mean turbulent kinetic energy. Numerical results (triangle) and experimental results (square) [12]. (a) $x = 7.27m$, (b) $x = 7.88m$. The vertical coordinate is $Z = (z - \bar{\eta})/\bar{H}$ and the horizontal one is $K = \sqrt{\bar{k}}/(g\bar{H})$.

This numerical simulation does not produce results in good agreement with the numerical results in terms of time mean turbulent kinetic energy profiles, as shown in Fig. 4.

The production of turbulent kinetic energy, that is generated in the buffer layer and in the turbulent core, is not well predicted by this numerical model (configuration C2), because the first calculation grid cell for the turbulent kinetic energy is in the upper part of the turbulent core. For this reason the variability of the production of turbulent kinetic energy along the vertical direction cannot be taken into account.

The configuration C3 solves the turbulent kinetic energy equation and the motion equations also in the buffer layer to take into account the variability of the vertical distribution of turbulent kinetic energy and so the turbulent phenomena.

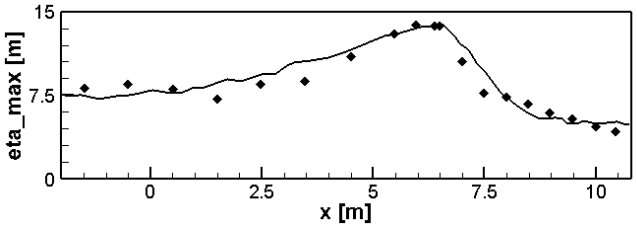

Fig. 5. Configuration C3: maximum water surface elevation. Numerical results solid line and experimental measurements (square) [12].

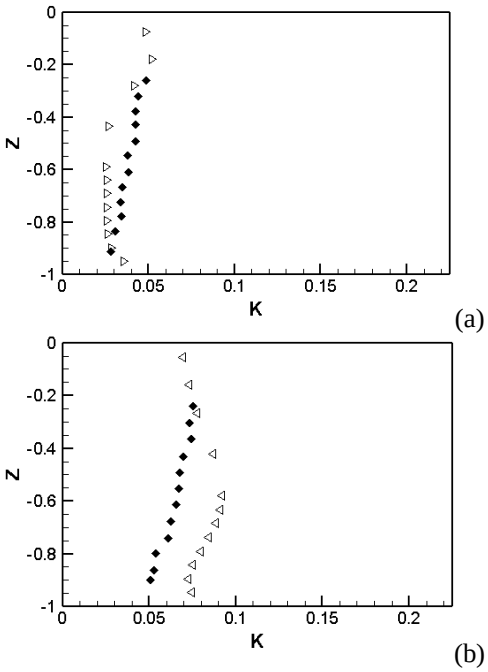

Fig. 6. Configuration C3: vertical distribution of the time mean turbulent kinetic energy. Numerical results (triangle) and experimental results (square) [12]. (a) $x = 7.27m$, (b) $x = 7.88m$. The vertical coordinate is $Z = (z - \bar{\eta})/\bar{H}$ and the horizontal one is $K = \sqrt{\bar{k}}/(g\bar{H})$.

The maximum water surface elevation and the time mean turbulent kinetic energy distribution along the vertical direction are in good agreement with the experimental results as it can see in Fig. 5 and Fig. 6. By placing the lower face at the first calculation grid cell at $y^+ = 10$ and by solving the al the equations in the buffer layer, the turbulent phenomena are well represented.

In Fig. 7 an instantaneous wave and velocity field is shown ($T = 100s$). One vector of each three is shown. In the zone after the breaking point the turbulent eddy viscosity, shown by the contour, is reduced by the use of the new formula for the mixing length.

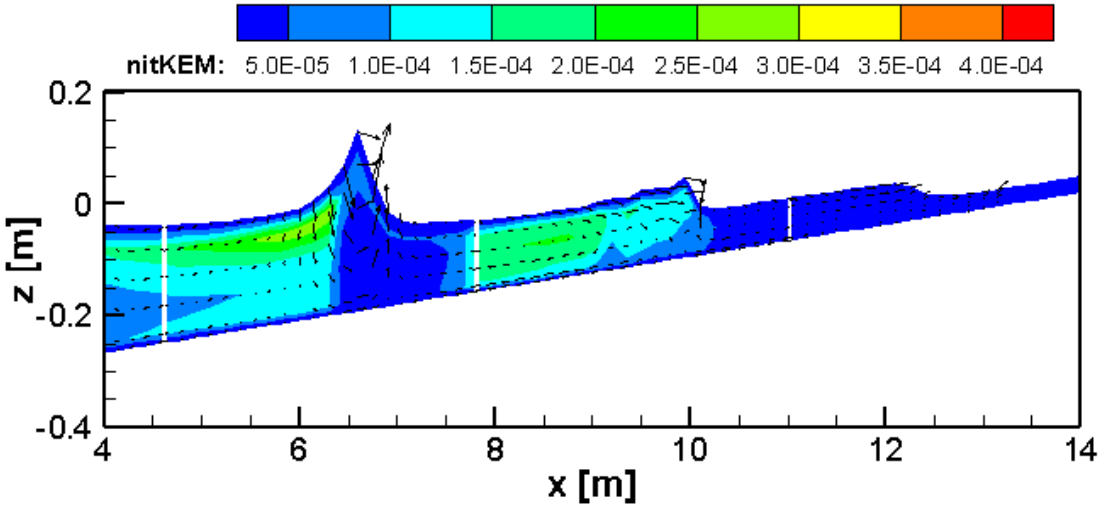

Fig. 7. Configuration C3: Instantaneous wave fields. Contour of turbulent eddy viscosity. Vector field in which one vectors of every three are shown. $T = 100s$.

5. Conclusion

In this paper a new $k-l$ turbulence model in contravariant form is proposed for three-dimensional simulation of breaking waves. In this model the mixing length is defined as a function of the first and second spatial derivatives of the maximum water surface elevation. It has been demonstrated that the new turbulence model, in which the motion equations and the turbulent kinetic energy equation are solve also in the buffer layer, produces results in good agreement with the experimental ones. The new model is able to represent the maximum water surface elevation and the time mean turbulent kinetic energy distribution along the vertical direction

References

[1] G. Ma, F. Shi, J.Y. Kirby, "Shock-capturing non-hydrostatic model for fully dispersive surface wave processes", Ocean Model, vol. 43-44, pp. 22-35, 2012.

[2] G. Cannata, C. Petrelli, L. Barsi, F. Gallerano, "Numerical integration of the contravariant integral form of the Navier–Stokes equations in time-dependent curvilinear coordinate systems for three-dimensional free surface flows", Contin. Mech. Thermodyn. vol. 31, pp. 491–519, 2019.

[3] B. Iele, F. Palleschi, "Boundary conditions for the simulation of wave breaking", WSEAS Transac. Fluid Mech., vol. 15, pp. 41-53, 2020.

[4] K.Z. Fang, Z.B Liu, "Modeling breaking waves and wave-induced currents with fully nonlinear Boussinesq equations", WSEAS Transac. Fluid Mech., vol. 9, pp. 131-143, 2014.

[5] F. Palleschi, B. Iele, F. Gallerano, "Integral contravariant form of the Navier-Stokes equations", WSEAS Transac. Fluid Mech., vol. 14, pp. 101-113, 2019.

[6] S. F. Bradford, "Numerical simulation of surf zone dynamics", J. Waterw. Port, Coast. Ocean Eng., vol. 126, pp. 1-13, 2000.

[7] F. Gallerano, G. Cannata, L. Barsi, F. Palleschi, B. Iele, "Simulation of wave motion and wave breaking induced energy dissipation", WSEAS Transac. Fluid Mech., vol. 14, pp. 62-69, 20191.

[8] G.Jiang, C. Shu, "Efficient Implementation of Weighted ENO Schemes", J. Comput. Phys., vol. 126, pp. 202-228, 1996.

[9] J. Peng, S. Liu, S. Li, K. Zhang, Y. Shen, "An efficient targeted ENO scheme with local adaptive dissipation for compressible flow simulation", J. Comput. Phys., vol. 425, pp. 1-25, 2021.

[10] F. Gallerano, G. Cannata, "Noll's axioms and formulation of the closure relations for the subgrid turbulent tensor in Large Eddy Simulation", WSEAS Transac. Fluid Mech., vol. 15, pp. 85-90, 2020.

[11] P.L.F. Liu, P. Lin, "A numerical model for breaking waves: the volume of fluid method", Res Report No. CACR-97-02, pp. 1-54, 1997.

[12] F.C.K. Ting, J.T. Kirby, "Observation undertow and turbulence in a wave period", Coast. Eng., vol. 24, pp. 177–204, 1995.

Contribution of Individual Authors to the Creation of a Scientific Article (Ghostwriting Policy)

The author(s) contributed in the present research, at all stages from the formulation of the problem to the final findings and solution.

Sources of Funding for Research Presented in a Scientific Article or Scientific Article Itself

No funding was received for conducting this study.

Conflict of Interest

The author(s) declare no potential conflicts of interest concerning the research, authorship, or publication of this article.